Numerical solution of atmospheric laser beam propagation using artificial compressibility and pseudo-spectral methods

Paulo Jorge Duda de Morais
University of São Paulo
São Paulo, Brazil
orcid.org/0000-0002-4336-2963

Rubens Cavalcante da Silva
University of São Paulo
São Paulo, Brazil
orcid.org/0000-0002-9794-0992

Wagner de Rossi
IPEN-CNEN/SP
São Paulo, Brazil
orcid.org/0000-0003-1371-7521

Claudio Costa Motta
University of São Paulo
São Paulo, Brazil
orcid.org/0000-0002-2508-7320

***Abstract*—In order to analyze the thermal blooming on wireless power transmission and remote recharge of batteries this study proposes a coupled numerical solution. The Navier-Stokes, energy and paraxial equations to the laser beam propagation through the atmosphere are solved by artificial compressibility and pseudo-spectral methods. Changes in the refractive index due to asymmetric temperature variations are the cause of this optical phenomenon. Numerical results are compared with reference studies and a good agreement is obtained. The conditions: laser beam, power density and absorptivity are constants; flow regime of $Re = 1000$, $Ri = 10.e4$, laser wavenumber $k = 10.e5$, and Stanton number $St = \frac{1}{30}$.**

***Index Terms*—thermal blooming, refractive index, paraxial equation, pseudo-spectral, artificial compressibility**

I. Introduction

Nowadays, the achievement of average power levels, on the order of multi kilowatts, of the silica optical fiber lasers, doped with rare earth ions, in particular the Yb^{3+} fiber laser, many technological applications have begun to show feasible. For example: medical surgeries, rock drilling, remote cloud sensing, radio astronomy, radio communication in space, satellite communication, wireless power transmission, remote laser communications, and lasers used to recharge batteries remotely. So, some of these applications are required an investigation of phenomena related to the atmospheric propagation of the laser beam [1], [2], [3] e [4]. Some recently researches started to model numerical solutions which the velocity field is a dynamic variable [5], in contrast with previews studies in that the fluid velocity had were prescribed [6], [7].

The effect known as thermal blooming occurs when a laser beam propagates through an absorbing medium. Although the absorption effect of the medium is very small, when the fluid is air, a change in the temperature and density fields in the vicinity of this laser beam is promoted. This temperature change induces a change in the refractive index and, with that, there is a loss of focus of the laser beam [6], [8]. The effect of thermal blooming has been discussed since the power of lasers became high enough to heat the medium, and the relevance of the phenomenon grows proportionally with increasing lasers power [9], [10] e [11].

In this work, the atmospheric effects on the propagation of high energy laser (HEL) will be conducted with emphasis on the heat generated due to the interaction of the laser beam and the consequent change in the refractive index [12].The scale of wavelengths and the distance of beam propagation differ by many orders of magnitude. So, the approach for the beam propagation will be done by using paraxial equation, [13], [14] like a envelope equation in axial direction. In order to include effects from the atmosphere the two dimensional uncompressible Navier-Stokes (N-S) equations will be used. The methodology to obtain the induced convection is the numerical solution of N-S equations in transversal direction with the method knowledge as artificial compressibility, first proposed by [15]. The laser beam propagation in axial direction will be described using spectral methods [16], such as fast Fourier transform (FFT) [17]. As a result, the "solver" will be a set of coupled N-S and wave paraxial equations and the Boussinesq approximation, to relate the dependence of the refractive index with the fluid temperature and velocity variations. The model in this work is based on the assumption that laser beam is the only source of energy in the environment, and it is large enough to neglect wind shear interference or air temperature fluctuations. But this power does not have the capability to change the properties of air at the molecular level.

This work is organized as follows: The first section is presented the formulation of the coupled beam and atmospheric dynamics; second section is presented the numerical methods; third section is shown simulations results. Finally, the last section presents few considerations on the results and the

978-1-6654-5273-1/22/$31.00 ©2022 IEEE

expectation of future works.

II. Formulation

In this section, it is presented the set of coupled wave paraxial and N-S equations which governs the propagation of the laser beam. The correlation between temperature T and refractive index η is done by the Boussinesq approximation for ideal gases (1) and Gladstone-Dale (2).

$$\frac{\rho_1}{\rho_0} = \frac{T_1}{T_0} \tag{1}$$

$$\eta_1 = (\eta_0 - 1)\frac{\rho_1}{\rho_0} \tag{2}$$

where ρ is the density, η_0 is the mean refractive index, η_1 is the correction of refractive index, T_0 is the mean temperature, T_1 is the correction of temperature.

Equations (1) and (2) are used to update refractive index in (3). The solution of paraxial equation is done by using the pseudo-spectral method. The core of this solution is the phase change in V, the electric field potential, across the axial direction.

$$\left(2ik\eta_0\frac{\partial}{\partial z} - \nabla^2 + 2\eta_0\eta_1 k^2\right)V = 0 \tag{3}$$

where, k is the wave-number in axial direction z. This equation has been numerically solved using the pseudo-spectral methods [18], [19].

These updates in V are then considered in the set of N-S equations to obtain the variables of fluid dynamics in transverse directions x and y. Hence, the only variable prescript in this model is the shape of the initial beam profile at $z = 0$:

$$V(x, y, z = 0, t) = e^{-(x^2+y^2)} \tag{4}$$

The set of equations that governs the fluid dynamics normally used in the literature is divided into groups characterized by the consideration of viscosity and compressibility in the phenomena of interest. One explanation of this division is the change in the mathematical character of the equations. In the case of compressibility, the compressible flow equations are hyperbolic. On the other hand, incompressible N-S equations have a mixed parabolic-elliptical character. This difference is a consequence of the absence of a time derivative term in the incompressible continuity equation. The core of the artificial compressibility method is to change the character of incompressible equations by including a time derivative pressure term with an artificial compressibility parameter [20]. This term at convergence is zero so the solution satisfies the incompressible equations. This approach was proposed by [15].

The artificial compressible unsteady N-S equations in the non-dimensional write:

$$\frac{1}{\gamma}\frac{\partial P}{\partial \tau} + \frac{\partial u}{\partial x} + \frac{\partial v}{\partial y} = 0 \tag{5}$$

$$\frac{\partial u}{\partial \tau} + \frac{\partial u}{\partial t} + u\frac{\partial u}{\partial x} + v\frac{\partial u}{\partial y} = -\frac{\partial P}{\partial x} + \frac{1}{Re}\left(\frac{\partial^2 u}{\partial x^2} + \frac{\partial^2 u}{\partial y^2}\right) \tag{6}$$

$$\frac{\partial v}{\partial \tau} + \frac{\partial v}{\partial t} + u\frac{\partial v}{\partial x} + v\frac{\partial v}{\partial y} = -\frac{\partial P}{\partial y} + \frac{1}{Re}\left(\frac{\partial^2 v}{\partial x^2} + \frac{\partial^2 v}{\partial y^2}\right) + RiTe_2 \tag{7}$$

$$\frac{\partial T}{\partial \tau} + \frac{\partial T}{\partial t} + u\frac{\partial T}{\partial x} + v\frac{\partial T}{\partial y} = \frac{1}{RePr}\left(\frac{\partial^2 T}{\partial x^2} + \frac{\partial^2 T}{\partial y^2}\right) + St|V|^2 \tag{8}$$

where u, v, P and T are the velocity in direction x, the velocity in direction y, scalar pressure and temperature fields, respectively.

As explained before, (5) has added the time derivative term of pressure in time scale τ, which is the pseudo-time and the parameter γ, which is the artificial compressibility. As a consequence, (6), (7) e (8) have two time derivative terms, one in the pseudo-time τ another in the time characteristic t. Where the numbers non-dimensional are: Reynolds (Re), Peclet (Pe), Richardson (Ri) and Stanton (St):

$$Re = \frac{UL}{\nu} \quad Pe = \frac{UL}{\mu} \quad Ri = \frac{gL}{U^2} \quad St = \frac{\beta V_0^2 L}{UT_0}$$

where, U is the velocity characteristic, L the lengthscale characteristic, β the absorbivity, $t = \frac{L}{U}$ the time characteristic, T_0 the temperature characteristic, V_0 beam intensity scale, g gravity, ν the kinematic viscosity, μ the thermal diffusivity, the characteristic pressure $P_0 = \rho_0 U^2$.

III. Simulation Setup

In order to obtain the numerical solutions of (5), (6), (7) e (8) in the time domain the fluid dynamics equations are solved in the transverse direction discretize in slices along the axial axis. To obtain a numerical solution for this system, the central finite differences technique was used to discretize the derivatives terms. The methodology for solving the system of equations was the artificial compressibility method. The basic idea of such method is to make the numerical iterations divided into two cycles. The first is to make the terms of the pseudo-time derivatives converge to zero and then use the results to obtain the next physical time of the N-S system.

A fourth-order Runge-Kutta scheme was used to obtain the solution on the scale of the pseudo-time. The parameter of numerical stability follows: to artificial compressibility [21], pseudo time discretization [22], physical time discretization [15] and spatial discretization.

After each interpolation, we use the fields of temperature do update refractive index, considering (1) e (2). Afterwards, the paraxial equation is solved in the pseudo spectral domain using FFT algorithm [17]. As a result, the laser beam amplitude update is obtained along the axial axis, with the update in η_1 as described in section II and the wave-number in the axial direction $k = 10^5$. A scheme of this system is showed in Fig. 1. The slices represent the points in axial direction where

the two dimensional N-S system is solved in the transverse direction, between these slices this model applies the paraxial equation with the update of the refractive index using the interpolation of temperature fields from the slices.

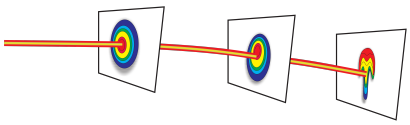

Fig. 1. Scheme of laser beam. The fluid is evolved according to N-S (5) - (8). The wave paraxial equation (3) is coupled by refractive index and Gladstone-Dale relationship (2). The beam deformation is due to differences in refractive index.

The simulations of N-S are developed considering a two-dimensional computational rectangular domain, $(x, y) \in (-2\pi, 2\pi) \times (-2\pi, 2\pi)$. The boundary conditions related to the computational domain are periodic to all components u, v, P, T. The initial conditions are the laser beam (4), temperature is initialized as $T(x, y, z, 0) = 0$ and velocity is initialized as $u(x, y, z, 0) = 0$ e $v(x, y, z, 0) = 0$. A staggered grid arrangement was implemented according to Fig. 2, the velocity components are located at points midway between the main grid nodes on the main node interfaces, the temperature components are located on the main grid nodes and the pressure components are located on the central of the volume limited by the main node interfaces.

For the grid, a two-dimensional isotropic mesh with a rectangular domain was used. The domain size was kept in a fixed non-dimensional space step of $h = 0.09$ and a non-dimensional fixed time step $\Delta t = 8 \times 10^{-4}$ was used.

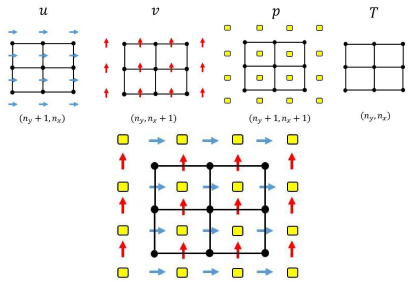

Fig. 2. Staggered Grid. Where the mesh components: blue arrows, red arrows, black dots and yellow squares are velocity u, velocity v, scalar pressure P and Temperature T

IV. Numerical Results

First, the set of non-dimensional numbers Re, Pe, Ri and St were kept fixed to analyze the numerical solution provided by the model in the development of the laser beam shape over time. As it is possible to see in (8), the Stanton number is the term responsible to couple the data from paraxial equation (3) with the set of Fluid-Dynamics. So it represents the power of the laser. As well the Richardson number represents the relation between natural convection and forced convection. In this simulation the set of dimensionless numbers utilized was $Re = 1000$, $Pe = 1000$, $Ri = 10.e4$ and $St = \frac{1}{30}$. For Fig. 3 to 5 the temperature fluctuations are reported in dimensional unit, degrees kelvin, $\eta_0 = 1.0003$, $T_0 = 300k$

Experiments since the 1970s have shown that, without wind, the crescent-shaped pattern is observed, but with a downward shift and a qualitative proof of how the distortion of the laser beam is caused by natural convection, [23]. This simulation used (3) and (5) to (8), with quiescent initial conditions and the laser beam profile give by (4). In the Fig. 3 is possible to see the temperature field starting to be developed (Fig. 3a), so the changes in the refractive index are small, as a result the distribution for the laser beam intensity is almost the same as the initial conditions, Fig. 3b.

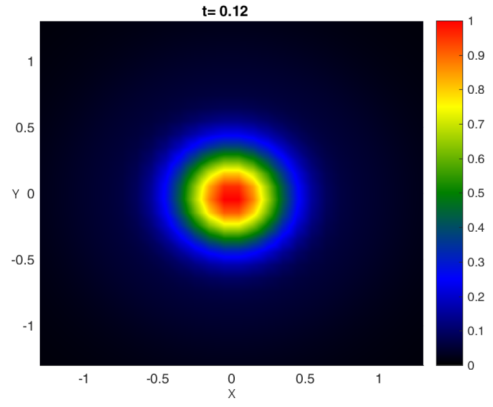

(a)

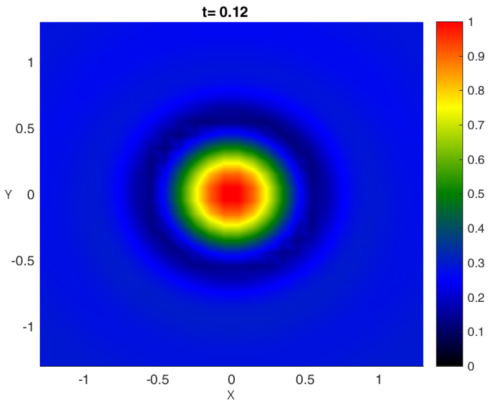

(b)

Fig. 3. Temperature fluctuations $T(x, y, z = 150, t = 0.12)$ (a) and laser beam intensity $|V|(x, y, z = 150, t = 0.12)$ (b). For these simulations $Re = 1000$, $Pe = 1000$, $Ri = 10.e4$ and $St = \frac{1}{30}$, the temperature fluctuations are reported in dimensional unit, degrees kelvin, $\eta_0 = 1.0003$, $T_0 = 300k$.

As the time progress, the forced convection due the warmer of fluid by the laser beam, started to create vortices which changed the radial symmetry of the temperature field, Fig. 4a, and the effects of the heating of the fluid make the change in the refractive index more significant, as consequence the shape in the laser beam intensity started to be changed, Fig. 4b.

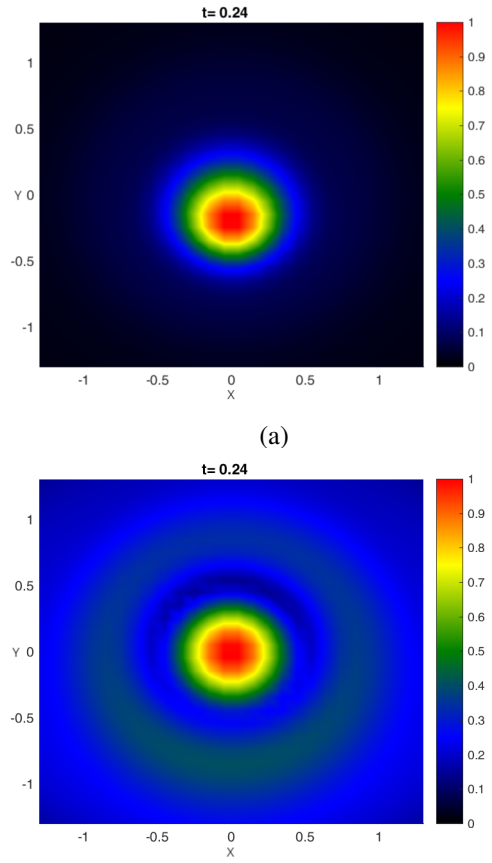

Fig. 4. Temperature fluctuations $T(x, y, z = 300, t = 0.24)$ (a) and laser beam intensity $|V|(x, y, z = 300, t = 0.24)$ (b). For these simulations $Re = 1000$, $Pe = 1000$, $Ri = 10.e4$ and $St = \frac{1}{30}$, the temperature fluctuations are reported in dimensional unit, degrees kelvin, $\eta_0 = 1.0003$, $T_0 = 300k$.

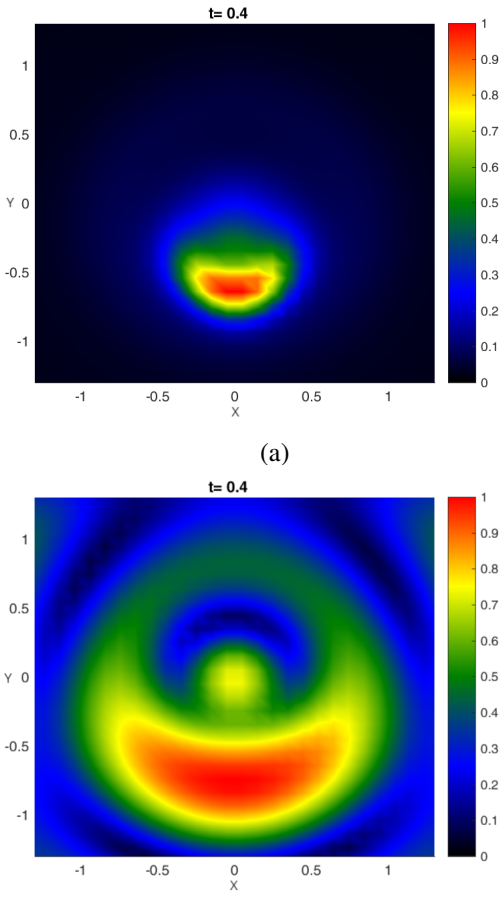

Fig. 5. Temperature fluctuations $T(x, y, z = 497, t = 0.4)$ (a) and laser beam intensity $|V|(x, y, z = 497, t = 0.4)$ (b). For these simulations $Re = 1000$, $Pe = 1000$, $Ri = 10.e4$ and $St = \frac{1}{30}$, the temperature fluctuations are reported in dimensional unit, degrees kelvin, $\eta_0 = 1.0003$, $T_0 = 300k$.

When the asymmetry of the temperature field is evident, Fig. 5a, the deformation of the laser beam intensity creates a crescent spread in the direction of forced convection, Fig.5b.

As expected, it is possible to observe in Fig. 5 how the numerical solution of this work represents the results obtained in the experiments, the effects of fluid heating and, as a consequence, the deformation of the laser beam. Over time, the fluid heats up and rises, and as a result, the beam deforms due to the resulting asymmetry in the refractive index. With the evolution of time, this effect is accentuated, promoting a distribution of the temperature field closer to the shape of a mushroom.

CONCLUSION

A numerical analysis of a gaussian laser beam atmospheric propagation was carried out. The thermal blooming effect was observed as the time evolved due to the effects of fluid heating and the consequent asymmetry of refractive index. Further improvement is being developed in the model to evaluate the effect of optical scintillation.

REFERENCES

[1] L. C. ANDREWS and R. L. Phillips, *Laser beam propagation through random media*, second edition ed. Bellingham: SPIE-International Society for Optical Engineering, 2005.

[2] D. E. Raible, D. Dinca, and T. H. Nayfeh, "Optical frequency optimization of a high intensity laser power beaming system utilizing VMJ photovoltaic cells," *2011 International Conference on Space Optical Systems and Applications, ICSOS'11*, pp. 232–238, 2011.

[3] N. Wang, Y. Zhu, W. Wei, J. Chen, S. Liu, P. Li, and Y. Wen, "One-to-multipoint laser remote power supply system for wireless sensor networks," *IEEE Sensors Journal*, vol. 12, no. 2, pp. 389–396, 2012.

[4] X. Liguan, "Wireless Power Transfer and Applications To Sensor Networks," *IEEE Wireless Communications*, no. August, pp. 140–145, 2013.

[5] J. S. Lane, "A Fixed-point Method for Computing Steady-state 2D Laser-Fluid Interactions," 2021.

[6] D. Smith, "High-power laser propagation: Thermal blooming," *Proceedings of the IEEE*, vol. 65, no. 12, pp. 1679–1714, 1977.

[7] J. Gustafsson, B. F. Akers, J. A. Reeger, and S. S. Sritharan, "Atmospheric propagation of high energy lasers," *Engineering Mathematics Letters*, 2019.

[8] S. J. Sheldon, L. V. Knight, and J. M. Thorne, "Laser-induced thermal lens effect : a new theoretical model," vol. 21, no. 9, pp. 1663–1669, 1982.

[9] D. Carroll, "Overview of High Energy Lasers: Past, Present, and Future?" in *42nd AIAA Plasmadynamics and Lasers Conference*. Reston, Virigina: American Institute of Aeronautics and Astronautics, 6 2011.

[10] M. D. Perry, D. Pennington, B. C. Stuart, G. Tietbohl, J. A. Britten, C. Brown, S. Herman, B. Golick, M. Kartz, J. Miller, H. T. Powell, M. Vergino, and V. Yanovsky, "Petawatt laser pulses," *Optics Letters*, vol. 24, no. 3, p. 160, 2 1999.

[11] Y. Sentoku, T. V. Liseikina, T. Z. Esirkepov, F. Califano, N. M. Naumova, Y. Ueshima, V. A. Vshivkov, Y. Kato, K. Mima, K. Nishihara, F. Pegoraro, and S. V. Bulanov, "High density collimated beams of relativistic ions produced by petawatt laser pulses in plasmas," *Physical Review E*, vol. 62, no. 5, pp. 7271–7281, 11 2000.

[12] F. G. Gebhardt, "Atmospheric Effects Modeling For High Energy Laser Systems Laser System Parameters Propagation Models : For Linear & Nonlinear Effects Target Irradiance Atmospheric Parameters , Scenario Geometry & Dynamics Performance Measures," vol. 2502, pp. 101–110, 1860.

[13] P. Sprangle, J. Peñano, and B. Hafizi, "Optimum wavelength and power for efficient laser propagation in various atmospheric environments," *Journal of Directed Energy*, vol. 2, no. 1, pp. 71–95, 2006.

[14] J. R. Penano, P. Sprangle, and B. Hafizi, "Propagation of high energy laser beams through atmospheric stagnation zones," *Navy Shipboard Lasers: Background, Advances, and Considerations*, pp. 71–86, 2015.

[15] A. J. Chorin, "A numerical method for solving incompressible viscous flow problems (Reprinted from the Journal of Computational Physics, vol 2, pg 12-26, 1997)," *Journal Of Computational Physics*, vol. 135, no. 2, pp. 118–125, 1997.

[16] D. Arsenović, J. Dimitrijević, and B. Jelenković, "Spectral method for numerical solution of the electric field envelope propagation equation," *Communications in Nonlinear Science and Numerical Simulation*, vol. 67, pp. 264–271, 2019.

[17] M. Frigo and S. Johnson, "FFTW: an adaptive software architecture for the FFT," in *Proceedings of the 1998 IEEE International Conference on Acoustics, Speech and Signal Processing, ICASSP '98 (Cat. No.98CH36181)*. IEEE, pp. 1381–1384.

[18] J. A. Fleck, J. R. Morris, and M. D. Feit, "Time-dependent propagation of high-energy laser beams through the atmosphere: II," *Applied Physics*, vol. 14, no. 1, pp. 99–115, 1977.

[19] R. Frehlich, "Simulation of laser propagation in a turbulent atmosphere," *Applied Optics*, vol. 39, no. 3, p. 393, 2000.

[20] J. H. Ferziger, M. Perić, and R. L. Street, *Computational Methods for Fluid Dynamics*. Cham: Springer International Publishing, 2020.

[21] W. W. Kim and S. Menon, "An unsteady incompressible Navier-Stokes solver for large eddy simulation of turbulent flows," *International Journal for Numerical Methods in Fluids*, vol. 31, no. 6, pp. 983–1017, 1999.

[22] P. Louda, K. Kozel, and J. Příhoda, "Numerical solution of 2D and 3D viscous incompressible steady and unsteady flows using artificial compressibility method," *International Journal for Numerical Methods in Fluids*, vol. 56, no. 8, pp. 1399–1407, 3 2008.

[23] F. G. Gebhardt and D. C. Smith, "Effects of wind on thermal defocusing of CO2 laser radiation," *Applied Physics Letters*, vol. 14, no. 2, pp. 52–54, 1969.